AGU PUBLICATIONS

JGR

Journal of Geophysical Research: Atmospheres

RESEARCH ARTICLE
10.1002/2017JD026683

Key Points:
- Significant regional differences exist in the occurrences of subdaily extreme rainfall in the U.S. during El Niño and El Niño Modoki
- Cold-season extreme rainfall occurrences in the U.S. respond more strongly to El Niño than to El Niño Modoki
- Their influences differ significantly in the Mountain States for the warm season and along the East/Gulf Coasts and CA for the cold season

Correspondence to:
S. Zhong,
zhongs@msu.edu

Citation:
Yu, L., S. Zhong, W. E. Heilman, and X. Bian (2017), A comparison of the effects of El Niño and El Niño Modoki on subdaily extreme precipitation occurrences across the contiguous United States, *J. Geophys. Res. Atmos.*, *122*, 7401–7415, doi:10.1002/2017JD026683.

Received 17 FEB 2017
Accepted 6 JUL 2017
Accepted article online 8 JUL 2017
Published online 26 JUL 2017

A comparison of the effects of El Niño and El Niño Modoki on subdaily extreme precipitation occurrences across the contiguous United States

Lejiang Yu[1,2], Shiyuan Zhong[2], Warren E. Heilman[3], and Xindi Bian[3]

[1]Key Laboratory for Polar Science of SOA, Polar Research Institute of China, Shanghai, China, [2]Department of Geography, Environment and Spatial Sciences, Michigan State University, East Lansing, Michigan, USA, [3]USDA Forest Service Northern Research Station, Lansing, Michigan, USA

Abstract Intense precipitation over a short duration is a major cause of flash floods. Using hourly rainfall data from the North America Land Data Assimilation System Phase 2 from 1979 to 2013, we compared the differences in the response of the subdaily extreme precipitation occurrences across the contiguous U.S. to strong anomalous warming over the eastern equatorial Pacific known as El Niño and over the central equatorial Pacific known as El Niño Modoki. For both types of anomalous equatorial Pacific warming, the teleconnection is much stronger in the cold season (November through April) than warm season (May through October). During the warm season, while both types correspond to an increase in subdaily extreme precipitation in areas of Texas and a decrease in some areas of the northern Plains, El Niño is associated with a significant increase in the northern Rockies and El Niño Modoki is associated with a decrease in the Intermountain West. During the cold season, the overall patterns are similar between the two types, with positive anomalies over much of the southern and negative anomalies over the northern U.S. However, large regional differences exist, with El Niño exerting a much stronger influence on subdaily extreme precipitation in the Atlantic and Gulf states as well as California, while the influence of El Niño Modoki is slightly broader over the Midwest. These differences can be largely explained by the vertical velocity, moisture convergence, and jet stream patterns induced by El Niño and El Niño Modoki episodes.

1. Introduction

Many areas of the United States (U.S.) are vulnerable to socioeconomic disruptions caused by extreme precipitation and resulting floods [*Easterling et al.*, 2000; *Spierre and Wake*, 2010; *Stevenson and Schumacher*, 2014]. Recent examples include the October 2015 South Carolina flooding resulting from a series of prolific rainfall events that shattered or surpassed countless records throughout the state causing 17 casualties and about $12 billion in damage [*Leberfinger*, 2015; *Mizzell et al.*, 2016], the August 2016 Louisiana flooding as extreme rainfall of more than 0.6 m fell over many areas sending rivers to record levels [*Watson et al.*, 2017], and the January–February 2017 California flooding as heavy rainfall associated with atmospheric rivers [*Rosen*, 2017] pounded the state threatening the safety of reservoir dams and causing record-setting flooding and mudslides [*Branson-Pott and Hamilton*, 2017]. Unfortunately, regions of the U.S. are likely to see more of these catastrophic flooding events as there has been an increasing trend over the recent decades in both the frequency and particularly the intensity of extreme precipitation, and this trend is likely to continue into the future [*Karl et al.*, 1995; *Karl and Knight*, 1998; *Kunkel et al.*, 1994, 1999, 2003, 2007; *Easterling et al.*, 2000; *Groisman et al.*, 2005, 2012; *Alexander et al.*, 2006; *Pryor et al.*, 2009; *Matonse and Frei*, 2013; *Muschinski and Katz*, 2013; *Horton et al.*, 2014; *Wuebbles et al.*, 2014; *Ning et al.*, 2015; *Yu et al.*, 2016].

Because of its significant socioeconomic impact, extreme precipitation and its relationships to large-scale atmosphere-ocean circulations have been the subject of many studies. Several studies have found that the variability of extreme precipitation in the U.S. is modulated by the interdecadal climate variability modes, such as the Pacific Decadal Oscillation (PDO), the North Pacific Index (NPI), and the Atlantic Multidecadal Oscillation (AMO). Over the contiguous U.S., the warm phase of the PDO is associated with an increase in wintertime extreme precipitation over the southern U.S. and a decrease in precipitation over the Great Plains, the Great Lakes, and the Ohio River Valley; the opposite occurs during its cold phase [*Zhang et al.*, 2010]. In the western U.S., *Deflorio et al.* [2013] found that during the warm (cold) phase of the PDO, cold-season extreme precipitation is more (less) intense in the southwestern than in the northwestern U.S. *Kenyon and Hegerl*

[2010] suggested that during positive phases of the NPI, the number of heavy precipitation events is reduced over the Pacific coast, the southwestern U.S., Texas, the High Plains, and Florida and increased over the Mountain West and the Ohio-Mississippi Basin. Florida and the coastal southeastern U.S. experience an increase in the intensity of warm-season (cold-season) precipitation during the warm (cold) phase of the AMO [*Curtis*, 2008; *Teegavarapu et al.*, 2013; *Goly and Teegavarapu*, 2014], with the increase in the warm-season precipitation intensity attributed to an increase in the number of major hurricanes during the AMO warm phase [*Goldenberg et al.*, 2001].

While the aforementioned decadal-scale, large-scale oscillations contribute to the variability of extreme precipitation in the U.S., subseasonal to interannual time scale oscillations, such as the El Niño–Southern Oscillation (ENSO), the North Atlantic Oscillation (NAO), and the Pacific-North American (PNA) pattern, also have a large influence on the frequency and intensity of extreme precipitation across the U.S. Several studies [e.g., *Goly and Teegavarapu*, 2014; *Carleton et al.*, 1990; *Griffiths and Bradley*, 2007; *Schubert et al.*, 2008, *Larkin and Harrison*, 2005] have shown that during El Niño years, wintertime daily heavy precipitation occurs more frequently over the central Rockies, the Gulf Coast, Florida, the Southwest, and the central U.S., while the Ohio/Mississippi River Valley and Red River Basin receive less wintertime extreme precipitation. The pattern is nearly reversed during La Niña years [*Gershunov and Barnett*, 1998; *Cayan et al.*, 1999; *Becker et al.*, 2009; *Higgins et al.*, 2010; *Schubert et al.*, 2008; *Shang et al.*, 2011; *Deflorio et al.*, 2013; *Goly and Teegavarapu*, 2014]. The relationship between ENSO and summertime daily extreme precipitation is less significant in many regions of the U.S. except over the northern Rockies where more (less) summertime extreme events occur during El Niño (La Niña) years [*Becker et al.*, 2009]. *Sun et al.* [2015] noted that the effect of ENSO on extreme precipitation in the U.S. is asymmetric and nonlinear in the central and western U.S., and symmetric in the southern U.S. The nonlinear relationship between ENSO and extreme precipitation is described in more detail by *Cannon* [2015] using two nonlinear statistical models. *Ning and Bradley* [2015a] examined the influence of ENSO, NAO, and PNA on wintertime extreme precipitation over the Northeast. They found that the wintertime precipitation response to ENSO agrees with the aforementioned studies. During positive phase PNA winters, more (less) extreme precipitation occurs over the western part of the Northeast (the Ohio River Valley). During positive phase NAO winters, more (less) extreme precipitation occurs over the southwestern part (the northern part) of the Northeast. The opposite occurs during the negative phase. But *Kenyon and Hegerl* [2010] and *Zhang et al.* [2010] noted only a weak response of extreme precipitation to the NAO.

Recent studies have identified a new El Niño pattern that is distinct from the conventional El Niño pattern defined as strong warm sea surface temperature (SST) anomalies in the eastern equatorial Pacific Ocean [*NOAA*, 2003]. The new El Niño pattern, also known as El Niño Modoki, is characterized by strong warm SST anomalies in the central equatorial Pacific Ocean sandwiched by cold SST anomalies over the tropical eastern and western Pacific Ocean [*Ashok et al.*, 2007; *Kao and Yu*, 2009]. In the case of El Niño, tropical convection is enhanced from the International Date Line to the eastern Pacific, and the response of the atmosphere resembles the negative phase of the Tropical Northern Hemisphere (TNH) pattern [*Yu et al.*, 2012]. During El Niño Modoki episodes, tropical convection is enhanced over the central Pacific with an atmospheric response pattern similar to the positive phase of the PNA teleconnnection [*Weng et al.*, 2007; *Mo*, 2010; *Yu et al.*, 2012; *Zou et al.*, 2014; *Yu and Zou*, 2013; *Zou et al.*, 2014; *Ning and Bradley*, 2015a]. Consequently, the impacts of El Niño and El Niño Modoki on U.S. weather and climate are very different [*Mo*, 2010; *Yu and Zou*, 2013; *Liang et al.*, 2014; *Liang et al.*, 2015].

Several recent studies have examined the different effects of El Niño and El Niño Modoki on temperature and precipitation over the U.S. [*Mo*, 2010; *Yu and Zou*, 2013], hydro-climatology over the Mississippi River Basin [*Liang et al.*, 2014], and the low-level jet over the central U.S. [*Liang et al.*, 2015]. In a recent study, *Ning and Bradley* [2015b] investigated the influence of the two types of El Niño on winter climate extremes in the eastern and central U.S. using archived daily climate data. Their results show that compared to the conventional tropical eastern Pacific El Niño, the tropical central El Niño usually brings less extreme precipitation amounts, fewer days with large precipitation amounts, and smaller amounts of maximum consecutive 5 day total precipitation around the Great Lakes and Ohio River Valley regions. In this study, we utilized hourly precipitation data to examine the impacts of the two types of El Niño on the frequency of subdaily extreme precipitation events during both the warm and cold seasons across the

contiguous U.S. Intensive rainfall events at the subdaily time scale can cause flash floods [*Georgakakos*, 1986]. The difficulty in forecasting the locations of these events and the amount of rainfall they produce can further exacerbate the adverse effects of these short-duration extreme precipitation events [*Ahren et al.*, 2005]. In a recent study, *Yu et al.* [2016] examined the trends in the frequencies of subdaily extreme precipitation events in the U.S. and found increasing trends in the central and eastern U.S. and generally decreasing trends over most of the western U.S. The current study focuses specifically on the teleconnections between subdaily extreme precipitation frequencies and SST anomalies in the eastern and in the central equatorial Pacific Ocean. Together, these and other similar studies will increase our understanding of the large-scale background climate conditions that are conducive to extreme precipitation events, which is critical for improving seasonal predictions of extreme precipitation probabilities and associated flash floods.

2. Data and Methods

Similar to *Yu et al.* [2016], extreme precipitation events in the contiguous U.S. were identified using hourly rainfall data from the North America Land Data Assimilation System Phase 2 (NLDAS-2), an atmosphere and land-surface hydrology data set covering central North America with a 1/8 degree mesh spanning January 1979 to the present [*Cosgrove et al.*, 2003]. The hourly precipitation data were generated by integrating a large amount of in situ and remote sensing precipitation data (e.g., the National Oceanic and Atmospheric Administration (NOAA)-Climate Prediction Center (CPC) daily and hourly rain gauge data [*Higgins et al.*, 1996, 2000], hourly Doppler Stage II radar precipitation data, satellite rainfall data [*Joyce et al.*, 2004]) and model reanalysis products (North American Regional Reanalysis [*Mesinger et al.*, 2006]) to drive an off-line land surface model.

In this study we consider extreme rainfall events spanning 1, 3, 6, 12, and 24 h in the warm (May through October) season and in the cold (November through April) season. For each of the two seasons, an extreme rainfall event is defined as an event when the accumulated rainfall amount over the specified time interval exceeds the 95th percentile of all events of the same duration in that season over 35 years (1979–2013). During each season, the total number of extreme rainfall events for the given length is used to explore its relationship with the two types of El Niño. NLDAS-2 precipitation data tend to capture the occurrence of extreme precipitation events but underestimate precipitation amounts during some very large precipitation events at some stations [*Luo et al.*, 2003]. But since we are interested in the interannual varibility of the occurrences of the extreme precipitation events defined above as local exceedances of the 95th percentile of all events of the same duration, it is unlikely that the known bias of underestimation in the amount of precipitation will have a significant impact on our results.

In this study, the nonconventional type of El Niño, defined as strong anomalous warming in the central tropical Pacific and cooling in the eastern and western tropical Pacific, is represented by the El Niño Modoki index obtained from the Japan Agency for Marine-Earth Science and Technology (http://www.jamstec.go.jp/frsgc/research/d1/iod/modoki_home.html.en). To represent the conventional El Niño characterized by strong anomalous warming in the eastern equatorial Pacific, SST anomalies in the Niño 3.4 region (bounded by 170°W–120°W and 5°S–5°N) are used, similar to the methodology adopted by *Trenberth* [1997], *Curtis et al.* [2007], and *Cannon* [2015], although the Niño 3 region (150°W–90°W and 5°S–5°N) is more representative of the eastern equatorial Pacific. The Niño3.4 index data were obtained from the NOAA-CPC (http://www.cpc.ncep.noaa.gov/data/indices/).

The corresponding large-scale atmospheric circulation patterns to El Niño and El Niño Modoki are derived using the gridded global reanalysis data produced by the National Centers for Environmental Prediction (NCEP) and the U.S. Department of Energy (DOE). These data have a temporal resolution of 6 h and a horizontal resolution of 2.5° latitude × 2.5° longitude [*Kanamitsu et al.*, 2002; *Kalnay et al.*, 1996]. In addition, the NOAA Extended Reconstructed SST data set [*Smith and Reynolds*, 2003, 2004] is also used for identifying the SST patterns over the Pacific Ocean.

The necessary condition for occurrence of extreme precipitation is a moisture-laden lower atmosphere. Using the NCEP-DOE global reanalysis, we can derive the vertically integrated low-level moisture fluxes for the warm or the cold seasons as follows [*Dominguez and Kumar*, 2005]:

$$qu = \frac{1}{g}\int_{1000\text{hPa}}^{500\text{hPa}} \overline{q}\overline{u}dp \quad (1)$$

$$qv = \frac{1}{g}\int_{1000\text{hPa}}^{500\text{hPa}} \overline{q}\overline{v}dp \quad (2)$$

where qu and qv are the zonal and meridional moisture flux components and $\overline{q}$, $\overline{u}$, and $\overline{v}$ are the seasonal mean specific humidity, zonal wind, and meridional wind at each pressure level, respectively.

In this study, we used regression analysis to investigate the effect of the two types of ENSO on U.S. subdaily extreme precipitation frequency. Apart from a single significant test at each grid point, a field significant test was also carried out to control the false discovery rate [*Wilks*, 2006, 2016].

3. Results

3.1. Spatial Patterns

We first discuss the climatological patterns of the number of extreme precipitation events for each of the five time intervals (1, 3, 6, 12, and 24 h) for the warm and the cold seasons. For each time interval, the warm- or cold-season climatological pattern, shown in Figure 1, is obtained by averaging the seasonal number of extreme precipitation events over the 35 year study period. The spatial patterns are substantially different between the two seasons. However, within each season, the spatial patterns remain very similar while the number of events decreases as the length increases from 1 to 24 h. Warm-season extreme precipitation events are much more frequent over the eastern U.S. than over the western U.S., with the highest numbers occurring in Florida and the lowest numbers occurring in California and the Intermountain West. Localized areas with large numbers are also found over high-elevation regions, particularly the Rocky Mountains, the Appalachians, and the Cascades, as convective lifting is enhanced by upslope flows. Cold-season extreme precipitation occurs predominantly in the Pacific Northwest particularly in western Washington and Oregon and over the Northern Rockies of Montana and northeastern Idaho. The occurrence of extreme wintertime precipitation in this region has been attributed to wintertime atmospheric rivers from the eastern Pacific Ocean [*Neiman et al.*, 2008]. In addition to the Northwest, the numbers of cold-season extreme precipitation events are also higher in the Great Lakes region and portions of the Northeast, while the numbers are lower over the central U.S. and the Southwest.

Significant seasonal differences also exist when the seasonal anomalies of the number of extreme precipitation events for each of the 35 warm and 35 cold seasons are regressed onto the time series of the seasonal Niño 3.4 and the El Niño Modoki indices over the same period (Figures 2 and 3). The warm-season El Niño regression map (Figure 2) shows significant positive anomalies over the northern Rockies and the southern Plains, an indication that more than the average number of extreme precipitation events in those areas occurs during El Niño episodes. Small areas of significant negative anomalies, indicating fewer events, are found in the northern Great Plains, Arizona, New Mexico, and the Northeast (Figure 2). The areal coverage of significant anomalies increases as the time interval increases from 1 to 24 h, but the overall response of the number of warm-season extreme precipitation events to El Niño episodes is weak. In contrast, El Niño appears to have a larger influence on the occurrences of cold-season extreme precipitation events as indicated by much broader areas with statistically significant anomalies compared to the warm season. There is a significant increase in the number of subdaily cold-season extreme precipitation events along the Gulf Coast, the Atlantic Coast, and areas of the Southwest and California. A significant decrease in the number of extreme precipitation events is found over the Ohio River Valley, Upper Midwest, and the Northwest.

The impact of El Niño Modoki episodes on the occurrence of subdaily extreme precipitation is clearly different from that of El Niño in both the warm and cold seasons. Most noticeably, the significant positive relationship between the warm-season extreme precipitation anomalies and El Niño episodes over the northern Rockies no longer exists for El Niño Modoki. Instead, significant positive connections are found over portions of Texas and the Southeast. Similar to El Niño, El Niño Modoki also has a stronger influence on the occurrences of extreme precipitation in the cold season than warm season. While the two types of El Niño result in minimal changes in the overall cold-season spatial regression patterns, the increase or decrease in the cold-season extreme precipitation occurrences is smaller during El Niño Modoki than during El Niño, as suggested by both smaller magnitude (both positive and negative) and smaller areas covered by

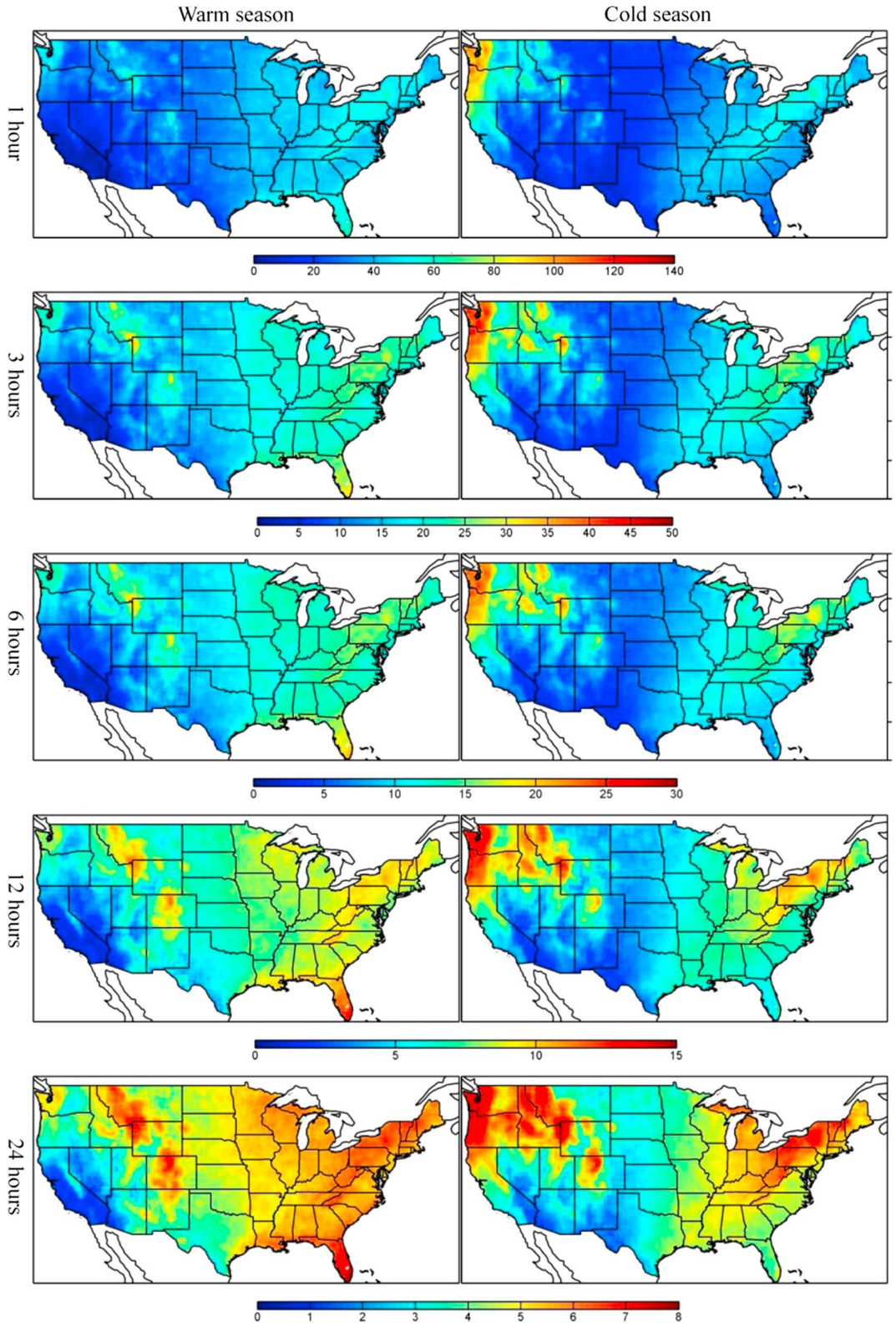

Figure 1. The 1979–2013 average number of extreme precipitation events for 1, 3, 6, 12, and 24 h duration for the warm and cold seasons.

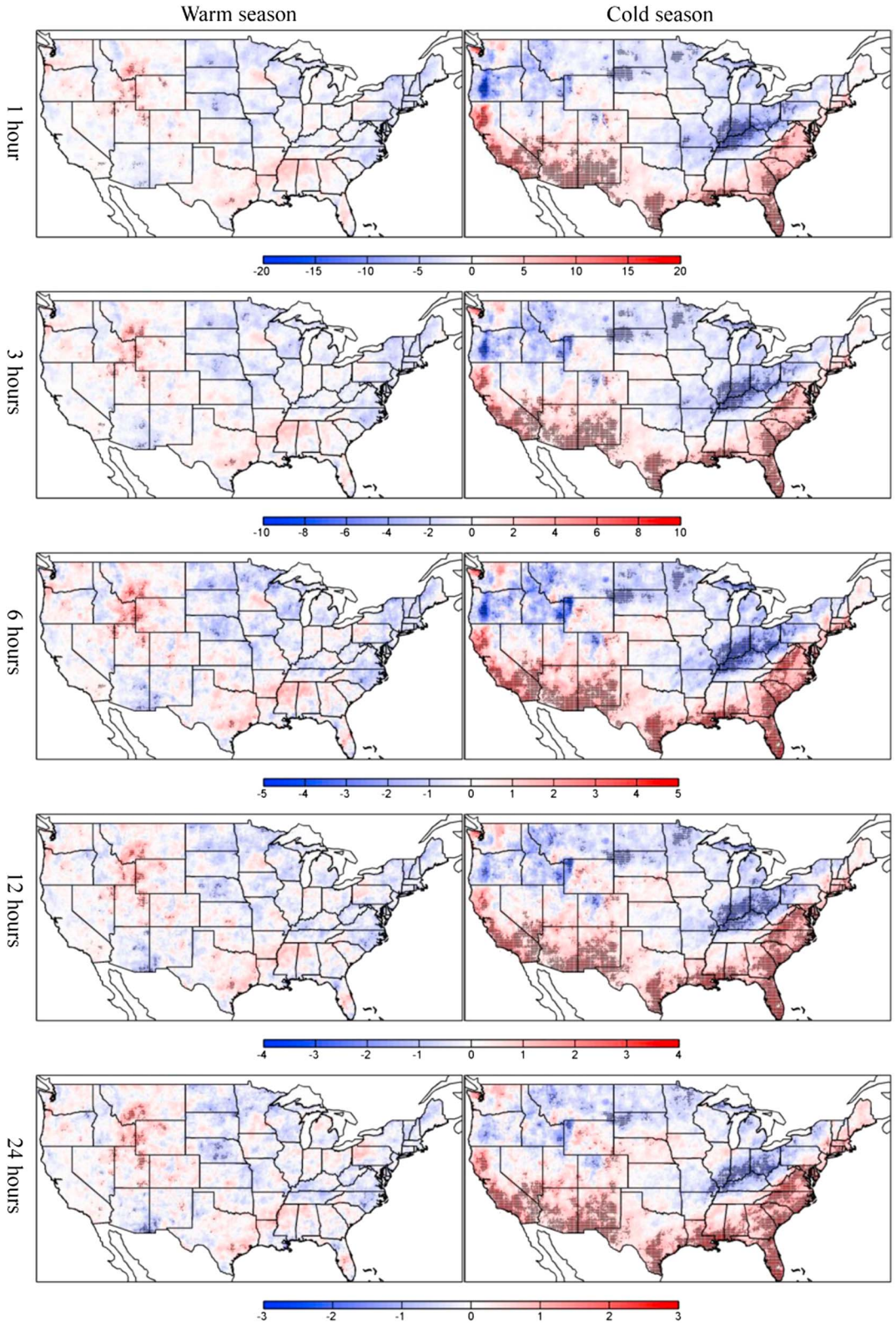

Figure 2. Anomalous warm- and cold-season number of extreme precipitation events with different durations regressed onto the normalized Niño 3.4 index. The dotted areas are globally significant at above 95% confidence level.

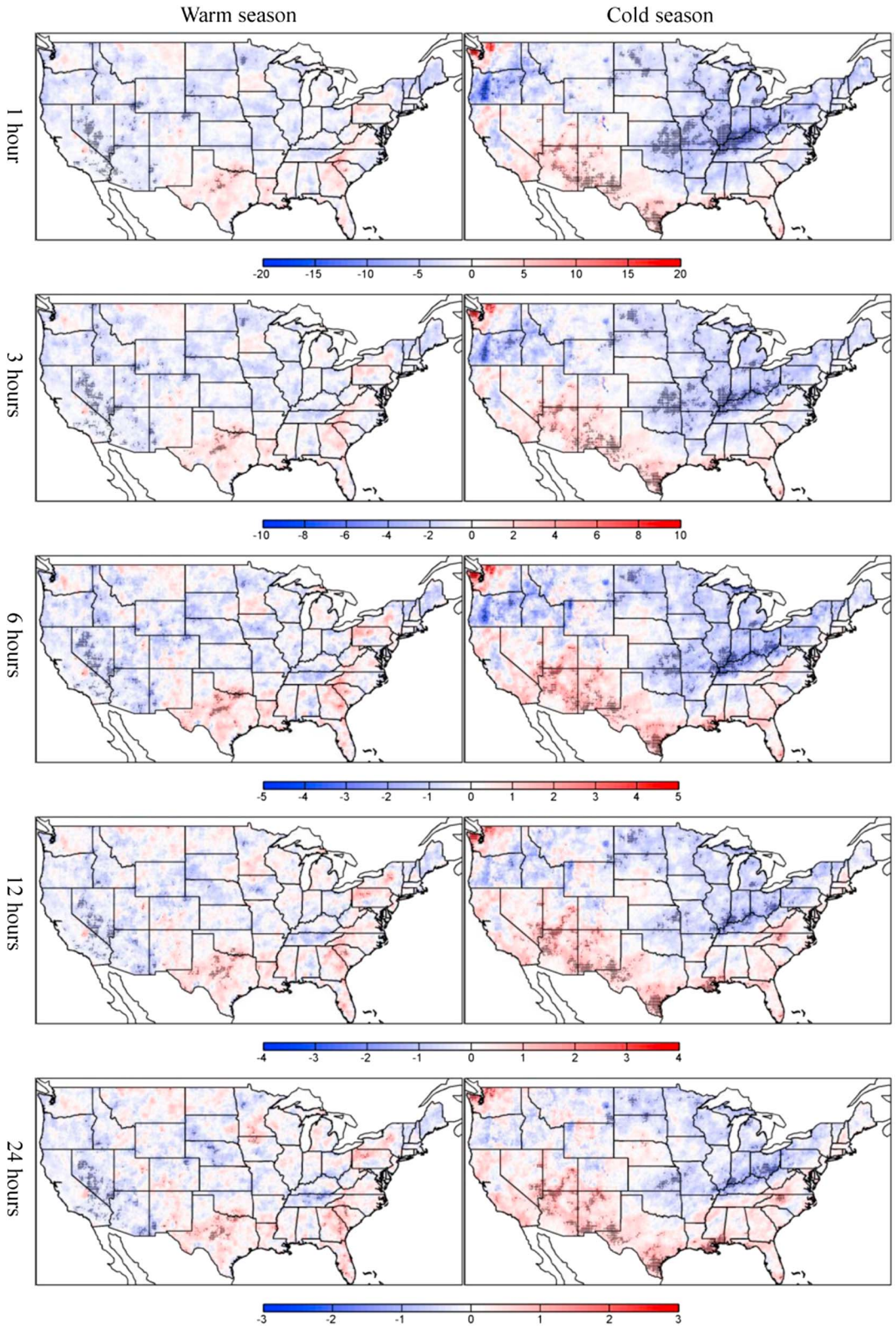

Figure 3. The same as Figure 2 but for the El Niño Modoki index.

Table 1. The Number of Grid Points With Statistically Significant Regression Coefficients Including Global Significance (Normal Font) and Without Global Significance (Bold Font) When the Extreme Precipitation Events of Different Durations Are Regressed Onto the Niño 3.4 (Figure 2) and El Niño Modoki (Figure 3) Indices

	El Niño Years				El Niño Modoki Years			
	Warm Season		Cold Season		Warm Season		Cold Season	
1 h	452	**1,123**	8,379	**10,657**	1,262	**2,257**	4,500	**7,505**
3 h	568	**1,236**	8,730	**10,923**	1,252	**2,151**	3,672	**6,520**
6 h	614	**1,365**	9,281	**11,406**	1,180	**2,066**	3,027	**5,530**
12 h	673	**1,423**	9,668	**11,806**	1,024	**1,885**	2,766	**4,985**
24 h	871	**1,765**	9,713	**11,839**	1,244	**2,202**	2,692	**4,815**

significant regression coefficients. For example, there is a statistically significant increase in the number of cold-season extreme precipitation events in the South Atlantic States and coastal California during El Niño, but this is not true during El Niño Modoki.

Except for small local differences, the overall spatial regression patterns remain nearly the same as the length of the events increases from 1 to 24 h for both seasons and both indices. However, for both seasons, the number of grid points with statistically significant (both field and global) regressions (dotted grid points in Figures 2 and 3), indicating an increase in the area of influence, increases with the length of the events for El Niño but generally decreases for El Niño Modoki (Table 1). The increased influence with duration during El Niño happened mostly during the warm season when the number of statistically significant points nearly doubled from 1 h to 24 h duration events. The decreased area of influence during El Niño Modoki occurs mostly during the cold season when there is a 40% decrease in the number of statistically significant points from 1 h to 24 h duration. During cold-season El Niño and warm-season El Niño Modoki years, no significant changes occur with the length of the events. *Kunkel et al.* [2012] and *Catto and Pfahl* [2013] noted that most of extreme precipitation events are associated with fronts. The opposite tendency of change in the number of significant grid points during different seasons may be related to the sensitivity of warm and cold front-induced precipitation to temporal scales [*Catto and Pfahl*, 2013].

From field to global significance (Table 1), the number of significant grid points decrease by 54% in the warm season and 20% in the cold season during El Niño years when averaged over events of all durations. During El Niño Modoki years the number is down by about 43% for both seasons. The decreases mainly occur in the western U.S. for the warm season and in the eastern U.S for the cold season.

3.2. Mechanisms

To elucidate the mechanisms underlying the different responses of the warm- and cold-season extreme precipitation events in the U.S. to El Niño and El Niño Modoki, we compare the spatial patterns of the anomalous 500 hPa geopotential heights, 200 hPa winds, and 850-hPa winds and moisture convergence regressed onto the Niño 3.4 index and the El Niño Modoki index, respectively. Previous studies [e.g., *Weng et al.*, 2007; *Mo*, 2010; *Yu et al.*, 2012; *Zou et al.*, 2014] have shown a close link between the anomalous circulation patterns at these levels and the climate of North America.

The regression maps of the warm-season 500 hPa height anomalies (Figures 4a and 4c) show similar spatial patterns over the North Pacific Ocean and North America. There are some noticeable differences along the Atlantic Coast where the below-normal heights corresponding to Niño 3.4 are replaced by above-normal heights with El Niño Modoki, suggesting that the latter is accompanied by a stronger Bermuda High. More significant differences are found between the spatial patterns for the cold season (Figures 4b and 4d). The pattern corresponding to Niño 3.4 (Figure 4b) bears resemblance to the negative phase of the TNH pattern [*Mo and Livezey*, 1986], with an elongated northwest-southeast oriented center of below-normal heights over the North Pacific including the Gulf of Alaska; below-normal heights over the southern U.S. the Gulf of Mexico, and the western North Atlantic; and above-normal heights over the north-central U. S. and much of Canada. The negative phase of the TNH pattern, which often occurs during El Niño, features increased precipitation over the southern U.S. especially the Southwest [*Weng et al.*, 2007; *Barnston et al.*, 1991]. The El Niño Modoki cold-season regression pattern (Figure 4d) shows above-normal heights over much of the western U.S. and below-normal heights over the eastern and portions of the southern U.S., which resembles the weak positive phase of the PNA pattern [*Yu et al.*, 2012]. For both indices, stronger SST anomalies over the tropical Pacific in the cold season produce more significant height anomalies over the North Pacific and North America than those in the warm season. The spatial patterns are also quite different between the warm and cold seasons.

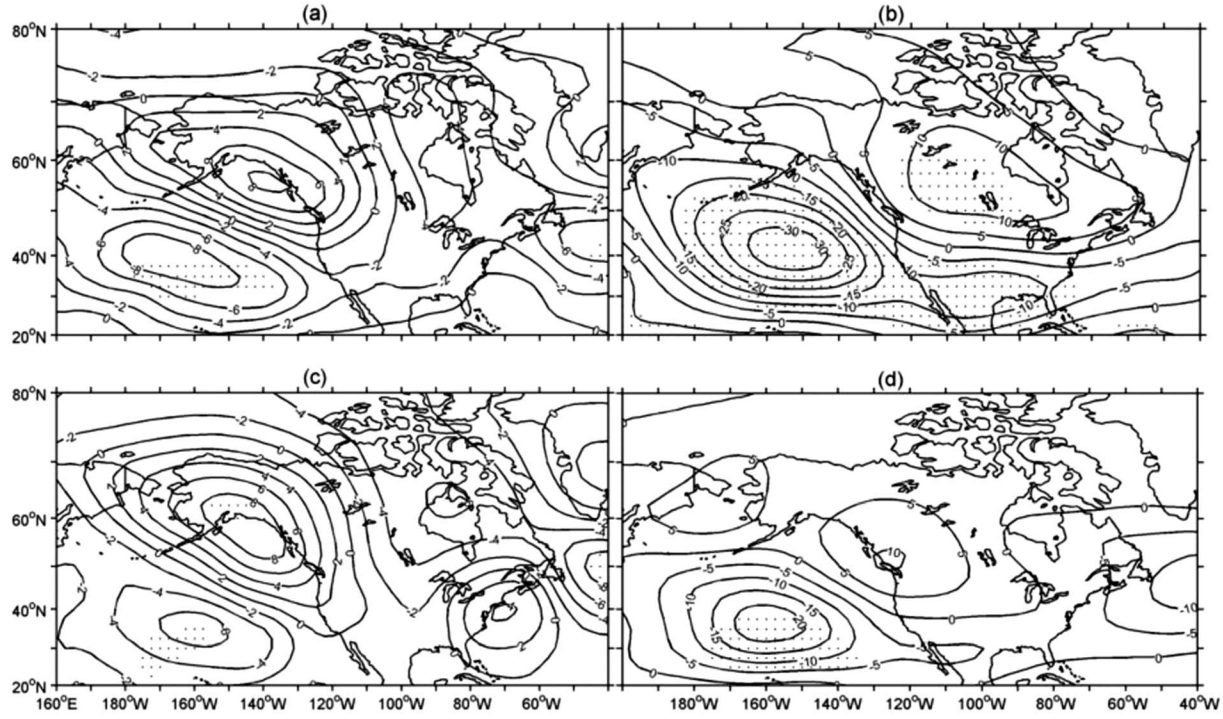

Figure 4. Anomalous 500 hPa geopotential height regressed onto the normalized (a and b) Niño 3.4 and (c and d) El Niño Modoki indices for the warm Figures 4a and 4c and the cold seasons Figures 4b and 4d. Globally, significant anomalies ($p < 0.05$) based on the two-tailed Student's t test are asterisked.

Seasonal differences also exist in the 850 hPa wind field regression patterns corresponding to the Niño 3.4 and the El Niño Modoki indices (Figure 5). Corresponding to Niño 3.4, the anomalous warm-season low-level northerly winds from southern Canada, the anomalous cyclone centered over Indiana and Ohio, and the anticyclone over Gulf of Mexico (Figure 5a) enhance moisture convergence over the southern U.S. and portions of the Midwest (Figure 6a), thus increasing the extreme precipitation probability in these regions (Figure 2, left column). Moisture convergence also occurs over the northern Rockies (Figure 6a), consistent with the positive extreme precipitation anomalies there. The negative anomalies of extreme precipitation in the north-central U.S. (Figure 2, left column) appear to be associated with anomalous northerly winds and moisture divergence there (Figure 6a). The cold-season pattern corresponding to Niño 3.4 shows anomalous cold and dry northeasterly winds and an anticyclonic cell over Canada and the eastern U.S. (Figure 5b), producing negative anomalies of extreme precipitation in the Northeast (Figure 2, right column). In contrast, anomalous warm, moist southwesterly winds and a cyclonic cell over the Southeast (Figure 5b) bring warm and moisture-laden air from the Atlantic and the Gulf of Mexico to the southern U.S. (Figure 6b), generating more extreme precipitation there. Anomalous moisture flux convergence also occurs over New Mexico and Texas States, while anomalous moisture flux divergence mainly occur over the northern U.S. (Figure 6b).

The warm-season 850 hPa wind field correspondence to the El Niño Modoki index features enhanced convergence over the Gulf Coast (Figure 6c) as the anomalous northerly winds extending from central Canada through the central U.S meet the anomalous southerly winds from the Gulf of Mexico (Figure 5c), a pattern favorable for extreme precipitation occurrence here (Figure 3, left column). The anomalous anticyclone over the western Atlantic (Figure 5c) also increases the moisture supply and the frequency of extreme precipitation in the southeastern U.S. (Figures 6c and 3, left column). However, anomalous northerly winds prevail across most of the western U.S., and the colder, drier air reduces the chance for the occurrences of extreme precipitation in this region. The cold-season 850 hPa wind field correspondence to the El Niño Modoki index shows an anomalous anticyclone over the Ohio River Valley and the Midwest (Figure 5d), which tends to weaken moisture convergence and reduce the chance for extreme precipitation events (Figure 3, right column). Meanwhile, the anomalous cyclonic cell over the Gulf of Mexico enhances the moisture supply and convergence along the Gulf Coast (Figure 6d).

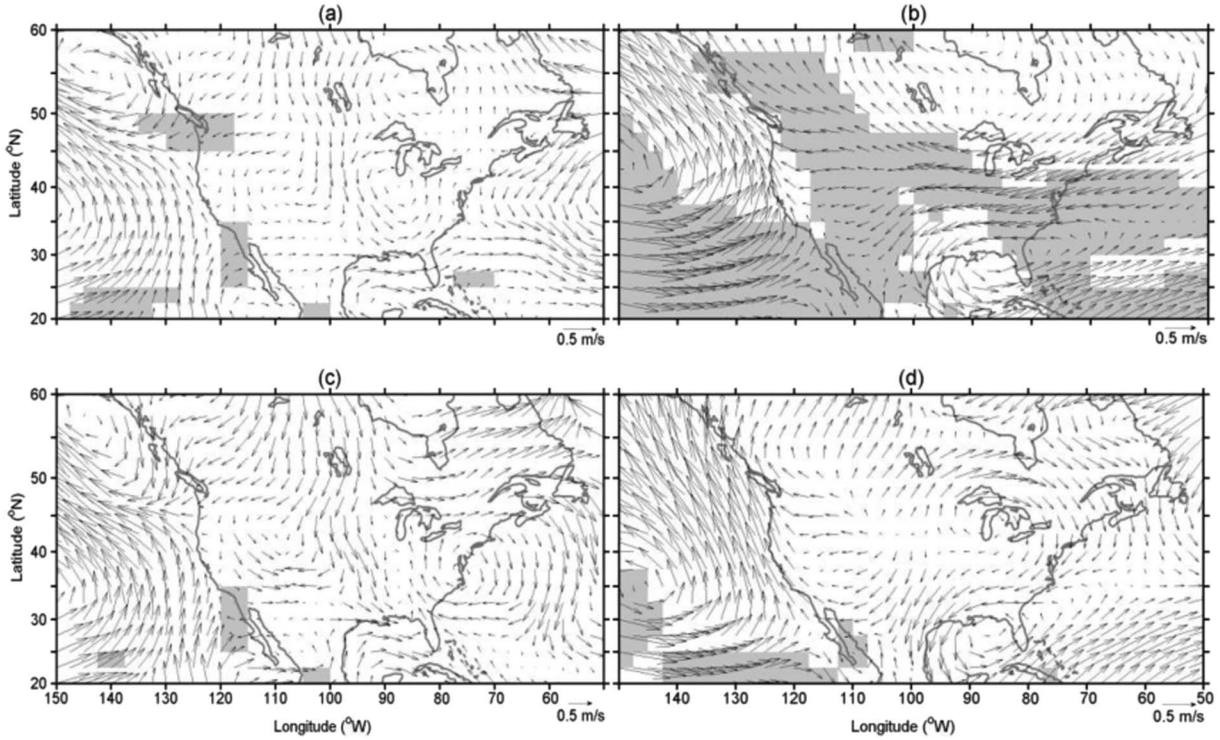

Figure 5. The same as Figure 4 but for 850 hPa wind field. Globally, significant anomalies ($p < 0.05$) based on the two-tailed Student's t test are shaded.

Apart from moisture transport, the atmospheric dynamics that lead to enhanced convection is also an important mechanism for extreme precipitation occurrence. Figure 7 shows regression patterns of the vertically averaged low-level (1000–500 hPa) anomalous omega fields (representing vertical motion) onto the Niño 3.4 index and the El Niño Modoki. The spatial patterns of rising and sinking motion correspond quite well with

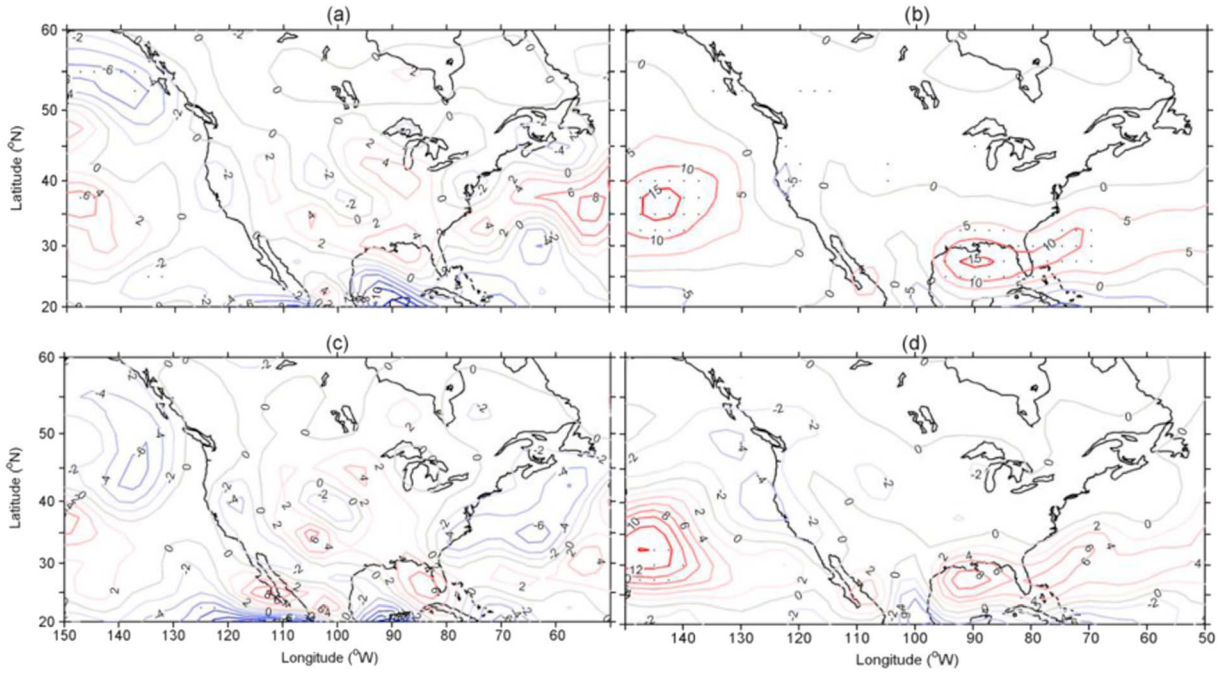

Figure 6. The same as Figure 4 but for low-level (1000–500 hPa) moisture convergence (unit: 10^{-7} g kg^{-1} s^{-1}). Positive (red) indicates moisture convergence, and negative (blue) indicates divergence. Globally, significant anomalies ($p < 0.05$) based on the two-tailed Student's t test are asterisked.

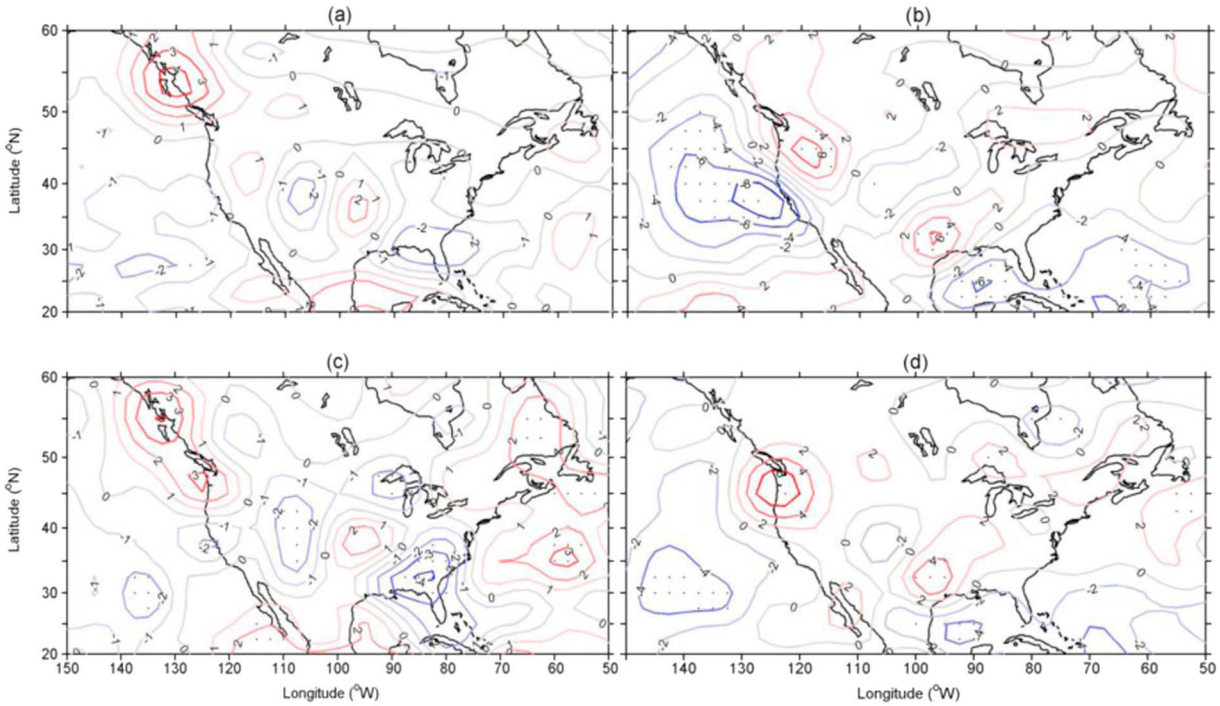

Figure 7. The same as Figure 4 but for low-level (1000–500 hPa) Omega field (unit: 10^{-3} Pa s^{-1}). Positive (red) indicates descending motion, and negative (blue) indicates ascending motion. Globally, significant anomalies ($p < 0.05$) based on the two-tailed Student's *t* test are asterisked.

the patterns of increased and decreased extreme precipitation frequency in Figures 2 and 3. The warm-season regression pattern for the Niño 3.4 index is characterized by anomalous upward motion over much of the Intermountain West and portions of the Southwest (Figure 7a), which helps lift water vapor to condensation levels, thus increasing the chances for extreme precipitation events. The anomalous sinking motion over the north-central and northeastern U.S. acts to suppress convection and reduce extreme precipitation occurrences. For the cold season, ascending motion along the Atlantic coast, portions of the Southeast, the Southwest, and west-central U.S. (Figure 7b) increase the chances for extreme precipitation events in these regions. Descending motion produces the opposite effect elsewhere in the U.S. (Figure 7b).

The warm-season omega field regression to the El Niño Modoki index shows strong anomalous rising motions over the Gulf Coast, the Southeast, and the Mid-Atlantic States, a condition conducive to more frequent extreme precipitation events (Figure 7c). The predominantly sinking motion over portions of the central Plains, the Southwest, and the Intermountain West decreases the likelihood of extreme precipitation in these regions. For the cold season (Figure 7d), sinking motions over the lower Midwest, the Northeast, and the Ohio River Valley favor less frequent extreme precipitation, while rising motions over the southern states increase the frequency there. A cell of strong anomalous sinking motion is seen over the Pacific Northwest, which explains the fewer number of extreme precipitation events across most of the region, except for western Washington where there are more cases of cold-season extreme precipitation events. This suggests that vertical motion may play a secondary role compared to moisture convergence (Figure 6d) when it comes to cold-season extreme precipitation in western Washington.

Catto and Pfahl [2013] and *Kunkel et al.* [2012] indicated that storm tracks are usually related to extratropical cyclones with frontal systems and these frontal systems and their associated atmospheric rivers are crucial for extreme precipitation events. *Athanasiadis et al.* [2010] suggested that jet stream patterns and related storm tracks are one of the most important factors affecting U.S. wintertime precipitation variability. Given this finding, we also investigated how El Niño and El Niño Modoki episodes affect cold-season jet stream patterns and associated cold-season extreme precipitation anomalies that contribute to the wintertime precipitation variability noted in *Athanasiadis et al.* [2010]. Figure 8 shows the regression maps of cold-season 200 hPa zonal winds onto the Niño 3.4 and El Niño Modoki indices. The general patterns are similar between the two,

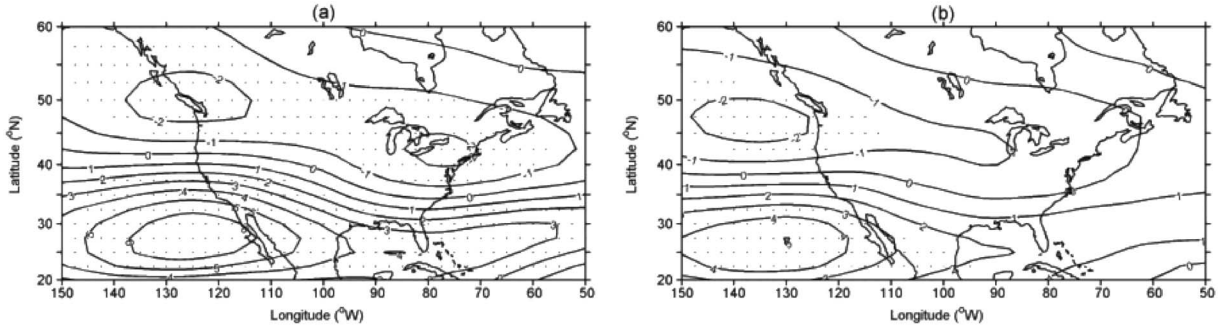

Figure 8. Anomalous cold-season 200 hPa zonal wind (unit: m s^{-1}) regressed onto the normalized (a) Niño 3.4 and (b) El Niño Modoki indices. Globally, significant anomalies ($p < 0.05$) based on the two-tailed Student's *t* test are asterisked.

with negative wind anomalies (indicating decreased zonal winds) over the north-central U.S. and positive anomalies over the southern U.S. However, the anomalous winds corresponding to the Niño 3.4 are stronger than the anomalous wind associated with the El Niño Modoki indices. The stronger zonal winds over the southern U.S. associated with El Niño lead to a more southern storm track, which generates more extreme precipitation events in the southern states compared to El Niño Modoki. The reduced zonal winds in central and northern U.S. and the southward displacement of the storm track lead to a general reduction in extreme precipitation occurrences over the central and northern U.S. under both conditions.

4. Summary and Discussion

This study examined the relationship between subdaily extreme precipitation occurrences across the contiguous U.S. and the different SST anomaly patterns over the equatorial Pacific Ocean associated with El Niño and El Niño Modoki episodes.

The results show that both El Niño and El Niño Modoki have a strong influence on the frequency of subdaily extreme precipitation events in the U.S., and the effect is much stronger on the cold-season than the warm-season frequency. For the warm-season extreme precipitation, statistically significant connections to the two types of El Niño are only found in small isolated areas. In particular, areas in the northern Rockies show an increase in frequency during El Niño episodes but not during El Niño Modok episodes. Areas of the Intermountain West experience a drop in the number of extreme precipitation events during El Niño Modoki but not during El Niño episodes. However, both produce an increase in subdaily extreme precipitation in areas of Texas and a decrease in some areas of the northern Plains. Cold-season extreme precipitation is more strongly connected to the two types of El Niño, with statistically significant positive anomalies over much of the southern U.S. and statistically significant negative anomalies over the northern U.S. Despite the similarity in the overall spatial patterns, there are large regional differences. Most noticeably, the significant positive anomalies over the Atlantic states and California associated with El Niño episodes are not present during El Niño Modoki episodes, while areas of significant negative anomalies associated with El Niño expand from the Ohio River Valley westward to the lower Midwest during El Niño Modoki episodes. Overall, the response of cold-season extreme precipitation occurrences is stronger to El Niño than El Niño Modoki. These general conclusions apply for extreme precipitation events with a time interval from 1 h to 24 h.

It is worth mentioning that our results of the impact of El Niño on 24 h extreme precipitation occurrences are consistent with previous studies using daily data [*Gershunov and Barnett*, 1998; *Cayan et al.*, 1999; *Becker et al.*, 2009; *Higgins et al.*, 2010; *Schubert et al.*, 2008; *Shang et al.*, 2011; *Deflorio et al.*, 2013; *Goly and Teegavarapu*, 2014]. As the length of the precipitation events shortens from daily to subdaily scales, some differences appear although the overall spatial patterns remain similar. In particular, the area of influence on cold-season extreme precipitation by El Niño Modoki tends to increase as the length of events decreases from 24 h to 1 h, but the area of influence on warm-season extreme precipitation by El Niño tends to decrease significantly as the length of the events shortens. In a recent study of the influence of the two types of El Niño on winter climate extremes in the eastern and central U.S., *Ning and Bradley* [2015b] presented a difference map

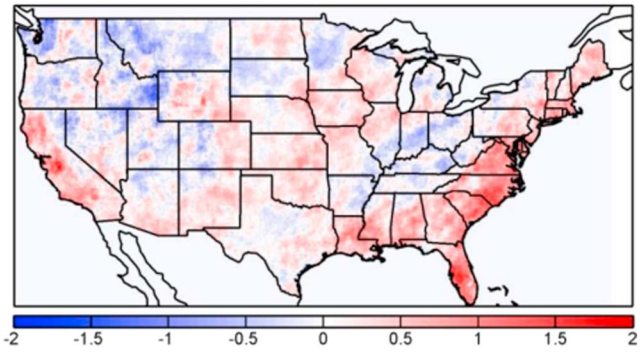

Figure 9. The differences of the anomalous number of cold-season daily extreme precipitation events regressed onto the normalized Niño 3.4 and El Niño Modoki indices.

(Figure 4a) between the composites of wintertime extreme daily precipitation during the eastern Pacific El Niño episodes and wintertime extreme daily precipitation during the central Pacific El Niño episodes. For comparison with their results, we show the difference of the regression maps of cold-season 24 h extreme precipitation between El Niño and El Niño Modoki years (Figure 9). Similar to their pattern, the differences are positive (indicating more events associated with El Niño episodes) over most of the Southeast, along the Atlantic Coasts and west of the Great Lakes. Differences are negative (fewer events associated with El Niño) extending from the Ohio River Valley to the Northeast. These differences can be explained by the differences in the strength of jet stream anomalies and the locations of the anomalous anticyclonic cell over the eastern U.S. The statistical relationship between the two types of ENSO and subdaily extreme precipitation in the U.S. can be used to help improve seasonal forecasts of subdaily extreme precipitation frequency based on Pacific SST anomalies.

As shown in previous studies, the planetary wave train pattern associated with El Niño episodes resembles that of the THN pattern, while the pattern associated with El Niño Modoki episodes is similar to that of the PNA pattern over the North Pacific and North America. Corresponding to the different wave train patterns, there are significant differences in the jet stream patterns, low-level wind fields, moisture convergence, and vertical motion between El Niño and El Niño Modoki years. Together they explain the differences in the occurrence of subdaily extreme precipitations events in different regions of the U.S.

The statistical relationships shown in this and other studies indicate that the SST anomalies over the tropical Pacific Ocean are a useful tool for anticipating where in the contiguous U.S. that extreme precipitation occurrences are more likely to be above or below normal, especially for SST anomalies associated with El Niño Modoki episodes that have become more frequent in recent decades [*Ashok et al.*, 2007]. Our results, however, did not consider the nonlinear response of U.S. extreme precipitation to the two types of ENSO. Previous studies have shown that there is a nonlinear relationship of precipitation, including extreme precipitation, to conventional El Niño [*Wu and Hsieh*, 2005, *Andrews et al.*, 2004; *Schubert et al.*, 2008; *Cannon*, 2015; and *Sun et al.*, 2015]. The possible nonlinear relationship between subdally extreme precipitation events and El Niño Modoki remains a topic for future studies. Moreover, it is worth noting that the relationships between the occurrences of extreme precipitation events in North America and the two types of El Niño, as outlined in this study, were established using a data set spanning only 35 years, which is a relatively short time period for comparing extreme precipitation occurrences with El Niño and El Niño Modoki oscillations that have a period of 2–7 years. The interdecadal climate modes (PDO and AMO) may strengthen or weaken these relationships, but longer time series are needed to validate these relationships. Numerical simulations are also necessary to fully understand the physical mechanisms and the atmospheric dynamics through which the SST anomalies in the central and eastern tropical Pacific Ocean influence extreme precipitation in the U.S. Finally, this study used Niño 3.4 to represent conventional El Niño following the traditional approach, while Niño 3 (90°W–150°W and 5°S–5°N) may be a better representation of the eastern equatorial Pacific. We repeated the regression analysis using Niño 3, and the results are similar to those with Niño 3.4.

Acknowledgments
The research was supported partially by the USDA Forest Service Northern Research Station under Research Joint Venture Agreement 16-JV-11242306-101 and by AgBioResearch of Michigan State University. All data necessary to evaluate and build upon the current work are available in the references and Web sites cited in the data section of the paper.

References

Ahren, M., R. S. Kovats, P. Wikinson, R. Few, and F. Matthies (2005), Global health impacts of floods: Epidemiologic evidence, *Epidemiol Rev.*, *27*, 36–46.

Alexander, L., et al. (2006), Global observed changes in daily climate extremes of temperature and precipitation, *J. Geophys. Res.*, *111*, D05109, doi:10.1029/2005JD006290.

Andrews, E., R. C. Antweiler, P. J. Neiman, and F. M. Ralph (2004), Influence of ENSO on flood frequency along the California coast, *J. Clim.*, *17*, 337–348.

Ashok, K., S. K. Behera, S. A. Rao, H. Weng, and T. Yamagata (2007), El Niño Modoki and its possible teleconnection, *J. Geophys. Res.*, *112*, C11007, doi:10.1029/2006JC003798.
Athanasiadis, P. J., J. M. Wallace, and J. J. Wettstein (2010), Patterns of wintertime jet stream variability and their relation to the storm track, *J. Atmos. Sci.*, *67*, 1361–1381.
Barnston, A. G., R. E. Livezey, and M. S. Halpert (1991), Modulation of southern oscillation-northern hemisphere mid-winter climate relationships by the QBO, *J. Clim.*, *4*, 203–217.
Becker, E. J., E. H. Berbery, and R. W. Higgins (2009), Understanding the characteristics of daily precipitation over the United States using the North American Regional Reanalysis, *J. Clim.*, *22*, 6268–6286.
Branson-Pott, H., and M. Hamilton (2017), Governor Brown declared state of emergency after storms causing flooding, erosion, and highway damages, Los Angeles Times, Jan. 23, 2017. [Available at http://www.latimes.com/local/lanow/la-me-ln-la-rain-monday-20170123-story.html.]
Cannon, A. J. (2015), Revisiting the nonlinear relationship between ENSO and winter extreme station precipitation in North America, *Int. J. Climatol.*, *35*, 4001–4014.
Carleton, A. M., D. A. Carpenter, and P. J. Weser (1990), Mechanisms of interannual variability of the southwest United States summer rainfall maximum, *J. Clim.*, *3*, 999–1015.
Catto, J. L., and S. Pfahl (2013), The importance if fronts for extreme precipitation, *J. Geophys. Res. Atmos.*, *118*, 10,791–10,801, doi:10.1002/jgrd.50852.
Cayan, D. R., K. T. Redmond, and L. G. Riddle (1999), ENSO and hydrologic extremes in the western United States, *J. Clim.*, *12*, 2881–2893.
Cosgrove, B. A., D. Lohmann, K. E. Mitchell, P. R. Houser, E. F. Wood, J. C. Schaake, A. Robock, C. Marshall, J. Sheffeld, and Q. Quan (2003), Real-time and retrospective forcing in the North American Land Data Assimilation System (NLDAS) project, *J. Geophys. Res.*, *108*(D22), 8842, doi:10.1029/2002JD003118.
Curtis, S. (2008), The Atlantic multidecadal oscillation and extreme daily precipitation over the US and Mexico during the hurricane season, *Clim. Dyn.*, *30*, 343–351.
Curtis, S., A. Salahuddin, R. F. Adler, G. J. Huffman, G. Gu, and Y. Hong (2007), Precipitation extremes eastimated by GPCP and TRMM: ENSO relationships, *J. Hydrometeorol.*, *8*, 678–689.
Deflorio, M. J., D. W. Pierce, D. R. Cayan, and A. J. Miller (2013), Western U.S. extreme precipitation events and their relation to ENSO and PDO in CCSM4, *J. Clim.*, *26*, 4231–4243.
Dominguez, F., and P. Kumar (2005), Dominant modes of moisture flux anomalies over North America, *J. Hydrometeorol.*, *6*, 194–209.
Easterling, D. R., G. A. Meehl, C. Parmesan, S. A. Changnon, T. R. Karl, and L. O. Mearns (2000), Climate extremes: Observations, modeling, and impacts, *Science*, *289*, 2068–2074.
Georgakakos, K. P. (1986), A generalized stochastic hydrometeorological model for flood and flash-flood forecasting: 2. Case Studies, *Water Resour. Res.*, *22*(13), 2096–2106.
Gershunov, A., and T. Barnett (1998), Interdecadal modulation of ENSO teleconnections, *Bull. Am. Meteorol. Soc.*, *79*, 2715–2725.
Goldenberg, S. B., C. W. Landsea, A. M. Mestas-Nuñez, and W. M. Gray (2001), The recent increase in Atlantic hurricane activity: Causes and implications, *Science*, *293*, 474–479.
Goly, A., and R. S. V. Teegavarapu (2014), Individual and coupled influences of AMO ENSO on regional precipitation characterictics and extremes, *Water Resour. Res.*, *50*, 4686–4709, doi:10.1002/2013WR014540.
Griffiths, M. L., and R. S. Bradley (2007), Variations of twentieth-century temperature and precipitation extreme indicatiors in the northeast United States, *J. Clim.*, *20*, 5401–5417.
Groisman, P. Y., R. W. Knight, and T. R. Karl (2012), Changes in intense precipitation over the central United States, *J. Hydrometeorol.*, *13*, 47–66.
Groisman, P. Y., R. W. Knight, T. R. Karl, G. C. Hegerland, and V. N. Razuvaev (2005), Trends in intense precipitation in the climate record, *J. Clim.*, *18*, 1326–1350.
Higgins, R. W., J. E. Janowiak, and Y. Yao (1996), A gridded hourly precipitation data base for the United States (1963–1993). NCEP/Climate Prediction Center Atlas No.1.
Higgins, R. W., W. Shi, E. Yarosh, and R. Joyce (2000), Improved United States precipitation quality control system and analysis. NCEP/Climate Prediction Center Atlas No. 7.
Higgins, R. W., V. E. Kousky, and P. Xie (2010), Extreme precipitation events in the south-central United States during May and June 2010: Historical perspective, role of ENSO, and trends, *J. Hydrometeorol.*, *12*, 1056–1070.
Horton, R. G., W. Easterling, R. Kates, M. Ruth, E. Sussman, A. Whelchel, D. Wolfe, and F. Lipschultz (2014), Ch. 16: Northeast, in *Climate Change Impacts in the United States: The Third National Climate Assessment*, edited by J. M. Melillo, T. C. Richmond, and G. W. Yohe, pp. 371–395, U.S. Global Change Research Program.
Joyce, R. J., J. E. Janowiak, P. A. Arkin, and P. Xie (2004), CMORPH: A method that produces global precipitation estimates from passive microwave and infrared data at high spatial and temporal resolution, *J. Hydrometeorol.*, *5*, 487–503.
Kalnay, E., et al. (1996), The NCEP/NCAR 40-year reanalysis project, *Bull. Am. Meteorol. Soc.*, *77*, 437–471.
Kanamitsu, M., W. Ebisuzaki, J. Woollen, S.-K. Yang, J. J. Hnilo, M. Fiorino, and G. L. Potter (2002), NCEP/DOE AMIP-II Reanalysis (R-2), *Bull. Am. Meteorol. Soc.*, *83*, 1631–1643.
Kao, H.-Y., and J.-Y. Yu (2009), Contrasting eastern-Pacific and central-Pacific types of ENSO, *J. Clim.*, *22*, 615–632.
Karl, T. R., and R. W. Knight (1998), Secular trends of precipitation amount, frequency, and intensity in the United States, *Bull. Am. Meteorol. Soc.*, *79*, 231–241.
Karl, T. R., R. W. Knight, D. R. Easterling, and R. Q. Quayle (1995), Indices of climate change for the United States, *Bull. Am. Meteorol. Soc.*, *77*, 279–292.
Kenyon, J., and G. C. Hegerl (2010), Influence of modes of climate variability on global precipitation extremes, *J. Clim.*, *23*, 6248–6262.
Kunkel, K. E., S. A. Changnon, and J. R. Angel (1994), Climatic aspects of the 1993 upper Mississippi River basin flood, *Bull. Am. Meteorol. Soc.*, *75*, 811–822.
Kunkel, K. E., K. Andsager, and D. R. Easterling (1999), Long-term trends in extreme precipitation events over the conterminous United States and Canada, *J. Clim.*, *12*, 2515–2527.
Kunkel, K. E., D. R. Easterling, K. Redmond, and K. Hubbard (2003), Temporal variations of extreme precipitation events in the United States: 1895–2000, *Geophys. Res. Lett.*, *30*(17), 1900, doi:10.1029/2003GL018052.
Kunkel, K. E., T. R. Karl, and D. R. Easterling (2007), A Monte Carlo assessment of uncertainties in heavy precipitation frequency variations, *J. Hydrometeorol.*, *8*, 1152–1160.
Kunkel, K. E., D. R. Easterling, D. A. R. Kristovich, B. Gleason, L. Stoecker, and R. Smith (2012), Meteorological casues of the secular variations in observed extreme precipitation events for the conterminous United States, *J. Hydrometeorol.*, *13*, 1131–1141.

Larkin, N. K., and D. E. Harrison (2005), Global seasonal temperature and precipitation anomalies during El Niño autumn and winter, *Geophys. Res. Lett.*, *32*, L16705, doi:10.1029/2005GL022860.
Leberfinger M. (2015), Reports: Historical South Carolina flooding kills 17. Accuweather Report, Oct. 8, 2015. [Available at http://www.accuweather.com/en/weather-news/live-rain-lashes-eastern-us-ma/52740263.]
Liang, Y.-C., M.-H. Lo, and J.-Y. Yu (2014), Asymmetric response of land hydroclimatology to two types of El Niño in the Mississippi River Basin, *Geophys. Res. Lett.*, *41*, 582–588, doi:10.1002/2013GL058828.
Liang, Y.-C., J.-Y. Yu, M.-H. Lo, and C. Wang (2015), The changing influence of El Niño on the Great Plains low-level jet, *Atmos. Sci. Lett.*, *16*, 512–517, doi:10.1002/asl.590.
Luo, L., et al. (2003), Validation of the North American Land Data Assimilation System (NLDAS) retrospective forcing over the southern Great Plains, *J. Geophys. Res.*, *108*(D22), 8843, doi:10.1029/2002JD003246.
Matonse, A. H., and A. Frei (2013), A seasonal shift in the frequency of extreme hydrological events in southern New York state, *J. Clim.*, *26*, 9577–9593.
Mesinger, F., et al. (2006), North American regional reanalysis, *Bull. Am. Meteorol. Soc.*, *87*, 343–360.
Mizzell, H., M. Malsick, and W. Tyler (2016), The historic South Carolina rainfall and major floods of October 1–5, 2015, *J. South Carolina Water Res.*, *3*(1), 2–7.
Mo, K. (2010), Interdecadal modulation of the impact of ENSO on precipitation and temperature over the United States, *J. Clim.*, *23*, 3639–3656.
Mo, K. C., and R. Livezey (1986), Tropical-extratropical geopotential height teleconnections during the Northern Hemisphere winter, *Mon. Weather Rev.*, *114*, 2488–2515.
Muschinski, T., and J. I. Katz (2013), Trends in hourly rainfall statistics in the United States under a warming climate, *Nat. Clim. Change*, *3*, 577–580.
Neiman, P. J., F. M. Ralph, G. A. Wick, Y.-H. Kuo, T.-K. Wee, Z. Ma, G. H. Talylor, and M. D. Dettinger (2008), Diagnosis of an intense atmospheric river impacting the Pacific northwest: Storm summary and offshore vertical structure observed with COSMIC satellite retrievals, *Mon. Weather Rev.*, *136*, 4398–4420.
Ning, L., and R. S. Bradley (2015a), Winter climate extremes over the northeastern United States and southeastern Canada and teleconnections with large-scale modes of climate variability, *J. Clim.*, *28*, 2475–2493.
Ning, L., and R. S. Bradley (2015b), Influence of eastern Pacific and central Pacific El Niño events on winter climate extremes over the eastern and central United States, *Int. J. Climatol.*, *35*, 4756–4770.
Ning, L., E. Riddle, and R. S. Bradley (2015), Projected changes in climate extremes over the northern United States, *J. Clim.*, *28*, 3289–3310.
NOAA (2003), NOAA gets U.S. consensus for El Niño/La Niña index, definitions, press release, Camp Springs, Md., 30 Sept. [Available at http://www.noaanews.noaa.gov/stories/s2095.htm.]
Pryor, S. C., J. A. Howe, and K. E. Kunkel (2009), Howspatially coherent and statistically robust are temporal changes in extreme precipitation in the contiguous USA?, *Int. J. Climatol.*, *29*, 31–45.
Rosen, J. (2017), California rains put spotlight on atmospheric rivers, *Science*, *355*(6327), 787, doi:10.1126/science.355.6327.787.
Schubert, S. D., Y. Chang, M. J. Suarez, and P. J. Pegion (2008), ENSO and wintertime extreme precipitation events over the contiguous United States, *J. Clim.*, *21*, 22–39.
Shang, H., J. Yan, and X. Zhang (2011), El Niño-Southern Oscillation influence on winter aximum daily precipitation in California in a spatial model, *Water Resour. Res.*, *47*, W11507, doi:10.1029/2011WR010415.
Smith, T. M., and R. W. Reynolds (2003), Extended reconstruction of global sea surface temperature based on COADS data (1854–1997), *J. Clim.*, *16*, 1495–1510.
Smith, T. M., and R. W. Reynolds (2004), Improved extended reconstruction of SST (1854-1997), *J. Clim.*, *17*, 2466–2477.
Spierre, S. G., and C. Wake (2010), Trends in extreme precipitation events for the northeastern United States 1948–2007 carbon solutions New England, Univ. of New Hampshire. [Available at http://amwa.net/galleries/climate-change/ 2010_NortheastExtremePrecip.pdf.]
Stevenson, S. N., and R. S. Schumacher (2014), A 10-year survey of extreme rainfall events in the central and eastern United States using gridded multisensor precipitation analyses, *Mon. Weather Rev.*, *142*, 3147–3162.
Sun, X., B. Renard, M. Thyer, S. Westra, and M. Lang (2015), A global analysis of the asymmetric effect of ENSO on extreme precipitation, *J. Hydrol.*, *530*, 51–65.
Teegavarapu, R. S. V., A. Goly, and J. Obeysekera (2013), Influences of Atlantic multidecadal oscillation on spatial and temporal variability of precipitation extremes, *J. Hydrol.*, *495*, 74–93.
Trenberth, K. E. (1997), The definition of El Niño, *Bull. Am. Meteorol. Soc.*, *78*, 2771–2777.
Watson, K. M., J. B. Storm, B. K. Breaker, and C. E. Rose (2017), Characterization of peak streamflows and flood inundation of selected areas in Louisiana from the August 2016 flood, *U.S. Geol. Surv. Sci. Invest. Rep., 2017–5005*, 26 pp., doi:10.3133/sir20175005.
Weng, H., K. Ashok, and S. K. Behera (2007), Impacts of recent El Niño Modoki on dry/wet conditions in the Pacific rim during boreal summer, *Clim. Dyn.*, *29*, 113–129.
Wilks, D. S. (2006), On "field significance" and the false discovery rate, *J. Appl. Meteorol. Climatol.*, *45*, 1181–1189.
Wilks, D. S. (2016), "The stippling shows statistically significant grid points": How research results are routinely overstated and overinterpreted, and what to do about it, *Bull. Am. Meteorol. Soc.*, *97*, 2263–2273.
Wu, A., and W. W. Hsieh (2005), The nonlinear patterns of North American winter temperature and precipitation associated with ENSO, *J. Clim.*, *18*, 1736–1752.
Wuebbles, D., et al. (2014), CMIP5 climate model analyses: Climate extremes in the United States, *Bull. Am. Meteorol. Soc.*, *95*, 571–583.
Yu, J.-Y., Y. Zou, S. T. Kim, and T. Lee (2012), The changing impact of El Niño on US winter temperatures, *Geophys. Res. Lett.*, *39*, L15702, doi:10.1029/2012GL052483.
Yu, J.-Y., and Y. Zou (2013), The enhanced drying effect of central-Pacific El Niño on US winter, *Environ. Res. Lett.*, *8*, 014019, doi:10.1088/1748-9326/8/1/014019.
Yu, L., S. Zhong, L. Pei, X. Bian, and W. E. Heilman (2016), Contribution of large-scale circulation anomalies to changes in extreme precipitation frequency in the United States, *Environ. Res. Lett.*, *11*, 044003, doi:10.1088/1748-9326/11/4/044003.
Zhang, X., J. Wang, F. W. Zwiers, and P. Y. Groisman (2010), The influence of large-scale climate variability on winter maximum daily precipitation over North America, *J. Clim.*, *23*, 2902–2915.
Zou, Y., J.-Y. Yu, T. Lee, M.-M. Lu, and S. T. Kim (2014), CMIP5 model simulations of the impacts of the two types of El Niño on the U.S. winter temperature, *J. Geophys. Res. Atmos.*, *119*, 3076–3092, doi:10.1002/2013JD021064.